AIAA JOURNAL
Vol. 31, No. 6, June 1993

Supersonic Flutter Analysis of Composite Plates and Shells

R. M. V. Pidaparti*
Purdue University at Indianapolis, Indianapolis, Indiana 46202
and
Henry T. Y. Yang†
Purdue University, West Lafayette, Indiana 47907

A high-precision doubly curved quadrilateral thin shell finite element is used for studying the supersonic flutter behavior of laminated composite plates and shells. The composite material property is included using classical lamination theory, and the supersonic aerodynamic effect is included using linearized piston theory. To reduce the number of degrees of freedom of the finite element aeroelastic system, the normal modes approach is adopted. Results are presented to illustrate the behavior of flutter characteristics for composite plates and curved panels, and composite cylindrical and conical shells. Parametric studies concerning the effects of boundary conditions, fiber orientation, degree of orthotropy, and flow angle on the flutter characteristics are presented for a series of selected examples. The accuracy, efficiency, and applicability of the present finite element method are demonstrated by illustrative examples, and, whenever possible, the results are compared to alternative solutions available in the literature.

Nomenclature

a = panel length
h = plate or shell thickness
L = length of the shell
m = longitudinal wave number
n = circumferential wave number
R = shell radius
β = freestream dynamic pressure parameter
β^* = nondimensional freestream dynamic pressure parameter
β^*_{cr} = critical nondimensional freestream dynamic pressure parameter
θ = fiber angle
λ = nondimensional eigenvalue
λ_{cr} = critical nondimensional eigenvalue
μ = aerodynamic damping parameter
ρ = mass density of plate or shell
ψ = flow angle
ω = frequency
ω^* = nondimensional frequency

I. Introduction

EARLY works on panel flutter were concerned mainly with conventional isotropic panels. The research progress and some of the references can be found, for example, in the text books by Fung,[1] Bisplinghoff and Ashley,[2] and Dowell.[3,4] Early reviews on panel flutter can be found, for example, in Refs. 5–6. Olson,[7] Sander, Bon, and Geradin,[8] Yang and Sung,[9] and Mei,[10] among others, studied the flutter of isotropic flat panels using the finite element method. Some studies were also devoted to the flutter of composite panels (see, among others, Refs. 11–16). Ketter[11] considered the effects of boundary conditions and fiber angle of panels on the flutter boundaries. Rosettes and Tong[12] applied a hybrid stress finite element method and used linearized piston theory to analyze the flutter of anisotropic cantilever plates. Their results indicate that flutter characteristics are strongly dependent on the composite fiber angle and anisotropy. Srinivasan and Babu[13] studied the panel flutter of cross-ply laminated composites by using the integral equations method. Lin, Lu, and Tam[14] used an 18 DOF high-precision triangular finite element to perform a flutter analysis of symmetrically laminated composite panels. Their studies included the effects of composite fiber angle, orthotropic modulus ratio, flow direction, and aerodynamic damping on the flutter boundaries. Sawyer[15] used the Galerkin method to study both the flutter and buckling problems of general laminated plates with simply supported boundary conditions. Oyibo[16] presented an analytical approach by combining classical plate theory and Ackeret's aerodynamic strip theory to study the flutter behavior of an orthotropic panel.

In the past, some studies were also devoted to the flutter characteristics of cylindrical and conical shells (see, for example, Refs. 17–26). Among these, some investigations focused on the application of the finite element method to linear flutter analysis, such as those given in Refs. 20–23. Ueda, Kobayashi, and Kihira[20] used a conical frustum finite element to study the flutter behavior of conical shells, and their results agreed well with experimental data. Bismarck-Nasr reported the results of the application of an axisymmetric shell finite element to study the flutter behavior of isotropic circular cylindrical shells[21] and conical shells.[22] Sunder, Ramakrishnan, and Sengupta[23] applied an axisymmetric ring finite element to perform a flutter analysis of three-ply laminated conical shells. Of those who used shell finite elements to study flutter characteristics of curved panels and shells, most reported the use of axisymmetric elements in the literature. For the purpose of more general application, it appears plausible to extend the conventional formulation for quadrilateral shell finite elements to include the effects of supersonic aerodynamic forces and laminated composite materials. With the use of such quadrilateral elements, the configuration of the shell is no longer limited to being axisymmetric, i.e., curved quadrilateral elements can be used to study the flutter behavior of arbitrary shells and curved panels with nonaxisymmetric rectangular configurations. Furthermore, it seems of interest to explore in depth the effects of different material properties, layup schemes, and various flow angles on the flutter behavior as there is a renewed interest in supersonic transport aircraft.

This paper presents an accurate and efficient high-precision quadrilateral shell finite element for the supersonic flutter analysis of laminated composite plates and shells. To establish

Received Sept. 12, 1992; revision received Dec. 11, 1992; accepted for publication Dec. 11, 1992.

*Associate Professor, Department of Mechanical Engineering, 723 W. Michigan Street. Member AIAA.
†Professor of Aeronautics & Astronautics and Dean of Engineering. Fellow AIAA.

the validity of the present formulation and computer program, flutter examples of composite plates and isotropic cylindrical and conical shells were first studied, and the results were compared with existing alternative solutions and experimental data. To illustrate and demonstrate the applicability of the present formulation and computer program, flutter examples of laminated composite cylindrical and conical shells, as well as curved quadrilateral panels, were studied. In these examples, parametric studies concerning the effects of boundary conditions, flow angles, fiber angles, and anisotropic properties on the flutter boundaries and modes are presented with physical explanations. For the composite cylindrical and conical shells selected, the relations between the fundamental natural frequencies (and their corresponding circumferential wave numbers) and the flutter frequencies (and their corresponding modes) are studied. The fiber orientation has an interesting effect on shifting the coalescent modes. To illustrate this phenomenon, the coalescences of modes are plotted for selected composite curved panels.

II. Formulation

A high-precision quadrilateral shell finite element[27] is extended to include the property of composite materials based on classical lamination theory and also to include the effect of supersonic flow based on linearized piston theory for the flutter analysis of laminated composite plates, shells, and curved panels. Some of the details of the element development are available in Ref. 27.

The shell finite element is quadrilateral in shape and has four nodal points with a total of 48 deg. of freedom. The element nodal displacement vector is given as

$$\{q\}^T = [u,\ u_\xi,\ u_\eta,\ u_{\xi\eta},\ v,\ v_\xi,\ v_\eta,\ v_{\xi\eta},\ w,\ w_\xi,\ w_\eta,\ w_{\xi\eta}] \tag{1}$$

where u, v, and w are the displacement components in three curvilinear directions, ξ, η, and z, respectively. Bicubic Hermitian polynomials are used to interpolate each of the displacement components. For example, the w displacement is expressed as

$$w(\xi,\eta) = \sum_{i=1}^{4} \begin{Bmatrix} f_1 \\ f_2 \\ f_3 \\ f_4 \end{Bmatrix}_i^T \begin{Bmatrix} w \\ w_\xi \\ w_\eta \\ w_{\xi\eta} \end{Bmatrix}_i$$

$$\begin{Bmatrix} f_1 \\ f_2 \\ f_3 \\ f_4 \end{Bmatrix}_i = \begin{Bmatrix} G_i(\xi) & G_i(\eta) \\ H_i(\xi) & G_i(\eta) \\ G_i(\xi) & H_i(\eta) \\ H_i(\xi) & H_i(\eta) \end{Bmatrix}_i \tag{2}$$

where i is the node number, and

$$G_i(\xi) = 0.25\ (-\xi_i\xi^3 + 3\xi_i\xi + 2)$$

$$H_i(\xi) = 0.25\ (\xi^3 + \xi_i\xi^2 - \xi - \xi_i)$$

Similarly, the u and v displacement shape functions are defined.

The strain-displacement relations are represented in terms of curvilinear coordinates. The laminated anisotropic behavior is included using classical lamination theory. The shell is made up of an arbitrary number of layers. Each layer is assumed to be orthotropic with its principal material axes at an angle to the local coordinate axes. The stress-strain relations for each layer are transformed to be written in terms of the reference coordinate system. The stress and moment resultants are then related to the middle surface strains and the changes of curvature as[28]

$$\begin{Bmatrix} N \\ M \end{Bmatrix} = \begin{bmatrix} A & B \\ B & D \end{bmatrix} \begin{Bmatrix} \epsilon \\ \kappa \end{Bmatrix} \tag{3}$$

The vector $\{N\}$ contains the resultant tangential forces, the vector $\{M\}$ contains the resultant moments, the vector $\{\epsilon\}$ contains the middle surface strains, the vector $\{\kappa\}$ contains the changes of curvature, and the coefficients in matrices $[A]$, $[B]$, and $[D]$ are given as

$$[A_{ij},\ B_{ij},\ D_{ij}] = \int_{-h/2}^{h/2} [Q_{ij}](1,\ z,\ z^2)\ dz \qquad (i,\ j = 1,\ 2,\ 3) \tag{4}$$

where $[Q_{ij}]$ is the 3×3 plane-stress stiffness matrix for each individual layer, and h is the total thickness of the plate or the shell.

The derivation of the aeroelastic equations is obtained using Hamilton's principle. A system of equations of motion for a nonconservative elastic system can be obtained using a variation of the form

$$\int_{t_1}^{t_2} \delta(T - U)\ dt + \int_{t_1}^{t_2} \delta W\ dt = 0 \tag{5}$$

where T is the kinetic energy, U is the potential energy of the system, and δW is the virtual work done by the aerodynamic forces acting on the structure from time t_1 to t_2.

The derivation of the mass and stiffness matrices can be obtained using the stationary principle of kinetic and potential energies, respectively. The details of the 48×48 stiffness and consistent mass matrices can be found in Ref. 27. The aerodynamic stiffness and damping matrices are derived by considering the virtual work done by the aerodynamic forces

$$\delta W = \int_A p\,\delta w\ dA \tag{6}$$

where A is the area of the element that the pressure is acting on.

Assuming a first-order, high Mach number (M_∞) approximation to the linear piston theory,[29,30] the aerodynamic pressure acting on a curved surface area dA is given by

$$p = \left[\beta \frac{\partial}{\partial \xi} + \mu \frac{\partial}{\partial t} - \frac{\beta}{2r\sqrt{(M_\infty^2 - 1)}} \frac{\partial}{\partial t}\right] w \tag{7}$$

with

$$\beta = \frac{2q}{\sqrt{(M_\infty^2 - 1)}}; \qquad \mu = \beta \frac{1}{V} \frac{M_\infty^2 - 2}{M_\infty^2 - 1} \tag{8}$$

where p is the freestream aerodynamic pressure, V is the freestream velocity defined as parallel to the ξ axis, q is the freestream dynamic pressure, and r is the radius of curvature of the shell element.

The aerodynamic virtual work can be written in terms of the element nodal vector as

$$\delta W = \{\delta q\}^T [k_a]\{q\} - \{\delta \dot{q}\}^T [c_a]\{\dot{q}\} \tag{9}$$

with

$$[k_a] = -\beta \int_A \{f\} \frac{\partial \{f\}^T}{\partial \xi}\ dA \tag{10}$$

$$[c_a] = \left(-\mu + \frac{\beta}{2r\sqrt{(M_\infty^2 - 1)}}\right) \int_A \{f\}\{f\}^T\ dA \tag{11}$$

where $\{\dot{q}\}$ denotes the time derivative of the nodal vector. The matrices $[k_a]$ and $[c_a]$ are known as the aerodynamic stiffness and damping matrices, respectively. The aerodynamic stiffness matrix $[k_a]$ is asymmetric, whereas the damping matrix $[c_a]$ is symmetric.

The aeroelastic system of equations for the structure is obtained by assembling the element matrices, which can be symbolized by capital letters as

$$[M]\{\ddot{Q}\} + [c_a]\{\dot{Q}\} + ([K] + [K_a])\{Q\} = 0 \tag{12}$$

The system of equations is solved as an eigenvalue problem by assuming $\{Q\}$ to be

$$\{Q\} = \{\bar{Q}\}\ e^{st} \tag{13}$$

where s is a complex number and $s = s_r + is_i$.

To reduce the aeroelastic system of equations, the normal modes approach is used. First, free vibration analysis is performed to obtain the natural frequencies and mode shapes. Then, using a sufficient number of lowest modes for the aeroelastic system, Eq. (12) can be reduced by premultiplying by $[\Phi]^T$ and postmultiplying by $[\Phi]$,

$$([\omega_s] + \overline{[K_a]})\{\bar{Q}\} = [\bar{k}]\{\bar{Q}\} \tag{14}$$

$$\overline{[K_a]} = [\Phi]^T[K_a][\Phi] \tag{15}$$

where $[\bar{k}]$ is a diagonal matrix containing complex eigenvalues $(\overline{k_r} + i\overline{k_i})$, the matrix $[\Phi]$ is the modal matrix constructed by retaining the selected lowest natural modes of the structure, and $[\omega_s]$ is a diagonal matrix containing the squares of the structural natural frequencies as diagonal elements.

The system of equations in Eq. (14) results in an eigenvalue problem corresponding to a given value of the dynamic pressure parameter β. If the aerodynamic damping factor μ is neglected, the flutter boundary is obtained when the two relative lowest eigenvalues coalesce to give a critical value of β_{cr}. When $\mu > 0$, the flutter solution is obtained when

$$\frac{\overline{k_i^2}}{\overline{k_r}} \geq \frac{\mu^2}{\rho D} \tag{16}$$

with

$$D = \frac{E_2 h^3}{12(1 - \nu_{12}^2)} \tag{17}$$

For isotropic materials, $E_2 = E$, and $\nu_{12} = \nu$.

When presenting the subsequent results, the following nondimensional parameters are used: $\beta^* = \beta a^3/E_2 h^3$; $\omega^* = \omega a^2\sqrt{\rho h/E_2 h^3}$; and $\lambda^2 = -\omega^2 - \mu\omega a^4/E_2 h^3$.

III. Results and Discussion

A general computer program was developed for the present composite shell finite element formulation as applied to supersonic panel flutter analysis. As part of the evaluation process, the natural frequencies and flutter solutions were first obtained for those composite plates and isotropic cylindrical and conical shells for which alternative solutions were available. For flat panels, the shell element was reduced from 48 to 16 DOFs by removing those degrees of freedom related to the curvatures. For every example, a convergence study was performed by computing the four lowest natural frequencies related to the flutter frequencies and observing their convergence trends while the meshes were being successfully refined. It was found that for the square plates and curved panels, the values for the four lowest frequencies converged at the 6×6 mesh level. For the cylindrical and conical shell examples, the four lowest frequencies converged at the 1×10 mesh level (one element in the circumferential direction and 10 elements in the longitudinal direction). Thus, a 6×6 mesh was used to model the square plates and the curved panels, and a 1×10 mesh was used to model a strip of the cylindrical and conical shells. All computations were carried out using a CYBER 205 vectorized supercomputer at Purdue University.

Table 1 Examples considered to illustrate the supersonic flutter behavior of laminated composite square plates

Example	Lay-up scheme	Boundary condition
1	Unidirectional	S.S. and clamped
2	$[0/90]_{2s}$	Clamped
3	$[0/90]$	Clamped
4	$[\pm\theta]_{2s}$	Clamped
5	$[\pm 45]_{2s}$	Clamped
6	$[0/90]_{2s}$	Clamped

Table 2 Comparison of flutter boundaries (λ_{cr} and β^*_{cr}) for a symmetrically $[0/90]_{2s}$ and unsymmetrically $[0/90]$ laminated boron-epoxy composite square plates with all edges clamped

	$[0/90]_{2s}$ layup		$[0/90]$ layup	
Reference	λ_{cr}	β^*_{cr}	λ_{cr}	β^*_{cr}
Integral equation method[13]	46.09	446	28.99	163
Series solution[13]	47.19	474	29.79	173
Plate element[33] (8×8 mesh)	46.89	471	—	—
Present (6×6 mesh)	46.80	472	31.46	194

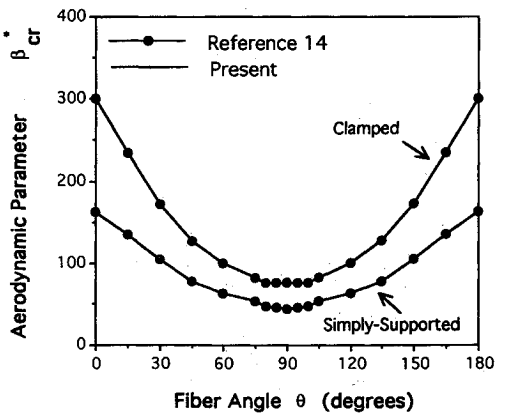

Fig. 1 Variation of critical flutter dynamic pressure parameter (β^*_{cr}) with fiber orientation for unidirectional composite ($E_1/E_2 = 5$, $G_{12} = 0.35\,E_2$, $\nu_{12} = 0.3$) square plates.

Composite Plates

The examples shown in Table 1 were first selected and studied systematically to illustrate the supersonic flutter behavior of laminated composite plates. Figure 1 shows the critical aerodynamic pressure parameter β^*_{cr} vs fiber orientation for a unidirectional composite plate with simply supported and clamped boundary conditions. The present results are compared to those of Ref. 14 using a 4×4, 18 DOF triangular element mesh, and excellent agreement is found. The aerodynamic pressure parameter is higher for the clamped plate than the simply supported plate for all the fiber orientations considered. For both plates, the aerodynamic parameter β^*_{cr} varies parabolically and symmetrically about the axial line at $\theta = 90$ deg, and the maximum and minimum values for β^*_{cr} are at $\theta = 0$ deg (or 180 deg) and 90 deg, respectively. In other words, for these two plates, maximum flutter speeds occur when the fiber composite angle is oriented along the direction of the flow, and minimum flutter speeds occur when the fiber angle is oriented perpendicular to the flow.

Table 2 shows the flutter bounds λ_{cr} and β^*_{cr} for a boron-epoxy $[(0/90)_2]_s$ and $[0/90]$ laminated composite plates with clamped boundary conditions. The material properties used for the boron-epoxy composite are $E_1 = 31 \times 10^6$ psi; $E_2 = 2.7 \times 10^6$ psi; $G_{12} = 0.75 \times 10^6$ psi; $\rho = 0.192 \times 10^{-3}$ lb-sec^2/in^4; and $\nu_{12} = 0.28$. The present finite element results are compared with other available solutions and experimental data in the table. It can be seen that the present results for the flutter bounds agree well with those given in Refs. 13 and 33. The present method is more efficient than the 45 DOF finite element in Ref. 33 because a smaller mesh (6×6) was used for this example. The present results for the $[0/90]$ case were different from those in Ref. 13, probably due to coupling stiffness caused by unsymmetrical layup and other factors such as consistent mass, etc., in the present finite element method.

Figure 2 shows the effect of fiber angle on the flutter bounds for a $[(\pm\theta)_2]_s$ angle-ply laminated composite square plate with all edges clamped. Figures 3 and 4 show the effect of flow direction on the flutter aerodynamic parameter (β^*_{cr}) and flutter eigenvalue (λ_{cr}) for a $[(\pm 45)_2]_s$ and a $[(0/90)_2]_s$ laminated composite plate with all edges clamped, respec-

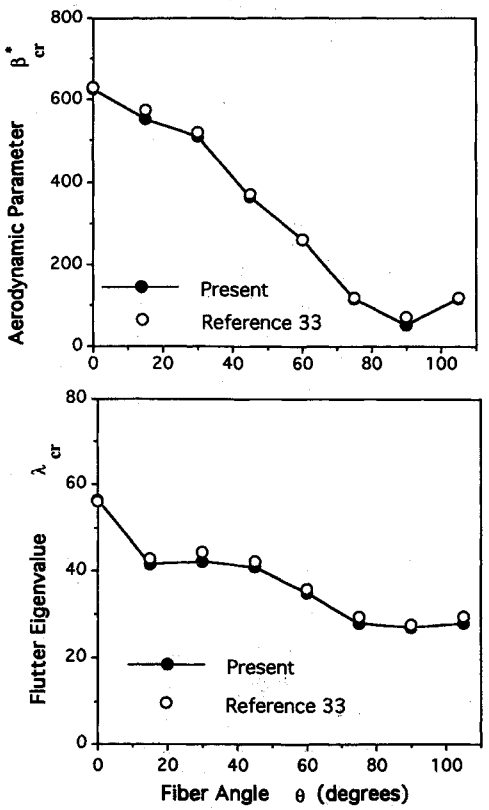

Fig. 2 Effect of fiber orientation on flutter boundaries (λ_{cr} and β^*_{cr}) for a $[(\pm\theta)_2]_s$ graphite-epoxy composite square plate with all edges clamped.

tively. All the results in Figs. 2–4 are compared to those by Lee and Cho[33] with good agreement. It is seen from Fig. 2 that, for the $[(\pm\theta)_2]_s$ angle-ply laminated plate, the values for β^*_{cr} decrease as the fiber angle increases from 0 deg to 90 deg, and the flutter frequency also decreases in the same fashion. Figure 3 shows that the maximum and minimum values for β^*_{cr} occur at flow angles of 45 deg and 0 deg (and 90 deg), respectively, for the $[(\pm 45)_2]_s$ laminated plate. Figure 4 shows that the maximum and minimum values of β^*_{cr} occur at flow angles of 0 deg and 90 deg, respectively, for the $[(0/90)_2]_s$ laminated plate. The flutter aerodynamic parameter for the $[(0/90)_2]_s$ laminated plate is 600 at a flow angle of 0 deg, which is significantly higher than that for the $[(\pm 45)_2]_s$ laminated plate. As the flow angle ψ increases, this difference narrows down and then reverses its trend after ψ becomes greater than approximately 45 deg.

Figure 5 shows the flutter mode shapes for the $[(0/90)_2]_s$ laminated composite plate for four different flow angles: 0 deg, 40 deg, 70 deg, and 90 deg, respectively. For the 40 deg, 70 deg, and 90 deg flow angles, flutter occurs when modes 1 and 2 coalesce. However, for the 0 deg flow angle, flutter occurs when modes 2 and 3 coalesce instead of modes 1 and 2. This interesting phenomenon seems to be due to the effect of composite material fiber orientation relative to the flow direction. Figures 2–5 have quantified the effects of fiber angles and flow directions on flutter characteristics such as flutter frequencies and modes for the present laminated composite plates.

Isotropic and Composite Shells

The examples shown in Table 3 were selected and studied systematically to illustrate the supersonic flutter behavior of isotropic and composite shells. An isotropic simply supported cylindrical shell of length $L = 40$ in., radius $R = 20$ in., and thickness $h = 0.04$ in., was first studied. The material properties were assumed as those for steel with $E = 30 \times 10^6$ psi; $\rho = 7.33 \times 10^{-4}$ lb-sec^2/in.^{4}; and $\nu = 0.3$. Figure 6 shows the results for flutter dynamic pressure parameter $\bar{\beta}$ and frequency $\bar{\omega}$ for the isotropic simply supported cylindrical shell as the number of circumferential waves (n) is increased from 9 to 30. The minimum value of the flutter speed (β^*_{cr}) occurs at $n = 16$. The present result obtained for the aerodynamic pressure parameter at $n = 16$ is compared to that by Kobayashi[19] with good agreement. The minimum $\bar{\omega}$ occurs at $n = 11$.

An isotropic simply supported conical shell with a 5 deg semivertex angle, and of length $L = 61.37$ in., radius $R = 7.55$ in., and thickness $h = 0.051$ in., was then studied. The material properties used are: $E = 6.5 \times 10^6$ psi; $\rho = 8.33 \times 10^{-4}$ lb-sec^2/in.^{4}; and $\nu = 0.29$. Table 4 shows the values of $\bar{\beta}^*_{cr}$ for four different values of n for this conical shell. The present flutter results are compared to those by an approximate method by Dixon and Hudson[31] and a conical frustum element solution by Ueda, Kobayashi, and Kihira[20] in Table 4. Reasonably good agreement is seen. The minimum value of β^*_{cr} occurs at $n = 5$ for this example.

Figure 7 shows the results of flutter boundaries for a graphite-epoxy $[0/\pm 45/90]_s$ laminated simply supported cylindrical shell for various circumferential wave numbers. The material properties used for the graphite-epoxy composite material are: $E_1 = 20 \times 10^6$ psi; $E_2 = 1.4 \times 10^6$ psi; $G_{12} = 0.8 \times 10^6$ psi; $\rho = 0.148 \times 10^{-3}$ lb-sec^2/in.^{4}; and $\nu_{12} = 0.3$. It is seen that as n is increased from 9 to 30, the critical flutter dynamic pressure parameter $\bar{\beta}$ decreases to a minimum at $n = 17$ and then increases. The flutter frequency $\bar{\omega}$ decreases to a minimum at $n = 11$ and then increases. It can be seen from Figs. 6–7 that the values of n that correspond to the lowest flutter aerodynamic pressures for the isotropic and composite shells are not necessarily the same but are very close due to the quasi-isotropic nature of the composite.

Figures 8–9 and 10–11 show the effect of fiber orientation on the two lowest frequencies, the flutter frequency and the dynamic pressure for a $[0/\pm\theta/90]_s$ and a $[(\pm\theta)_2]_s$ laminated simply supported cylindrical and conical shells, respectively. The material properties and geometry of the shell are similar to those used in Fig. 7. The circumferential wave numbers that correspond to the two lowest frequencies and the flutter fre-

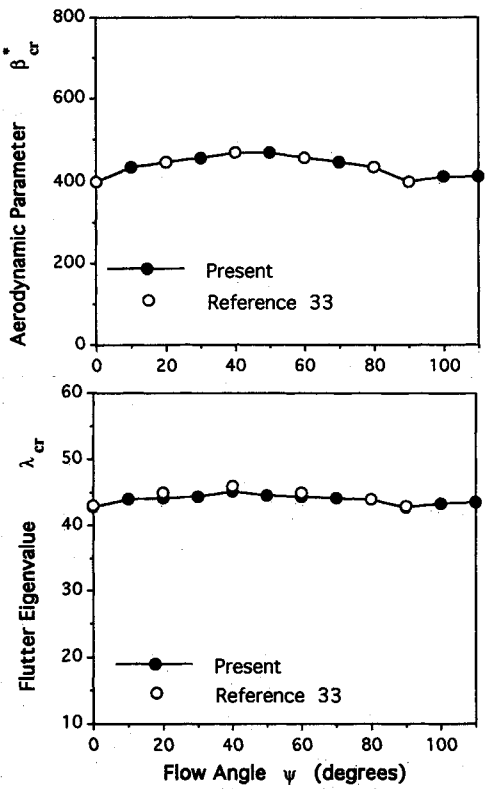

Fig. 3 Effect of flow direction on flutter boundaries (λ_{cr} and β^*_{cr}) for a $[(+45)_2]_s$ graphite-epoxy composite square plate with all edges clamped.

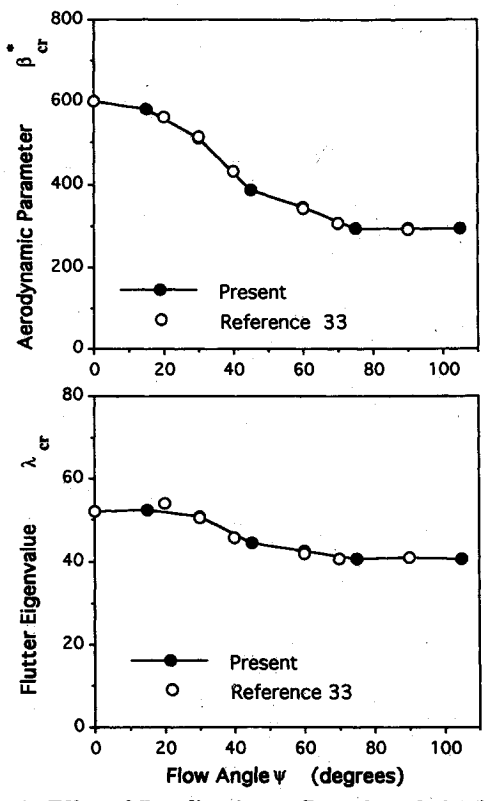

Fig. 4 Effect of flow direction on flutter boundaries (λ_{cr} and β^*_{cr}) for a $[(0/90)_2]_s$ graphite-epoxy composite square plate with all edges clamped.

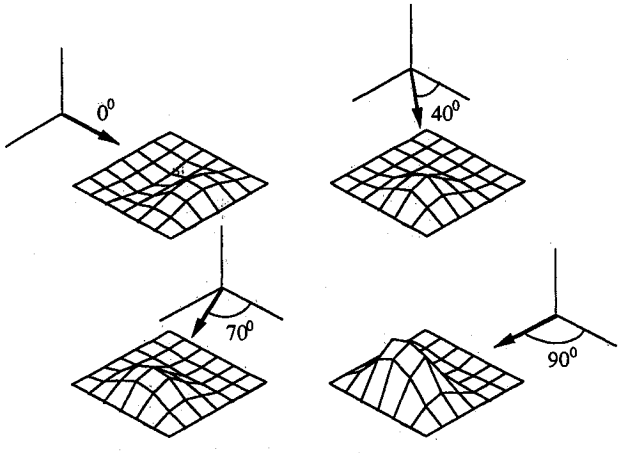

Fig. 5 Flutter mode shapes for the $[(0/90)_2]_s$ graphite-epoxy composite square plate at four different flow angles of 0 deg, 40 deg, 70 deg, and 90 deg.

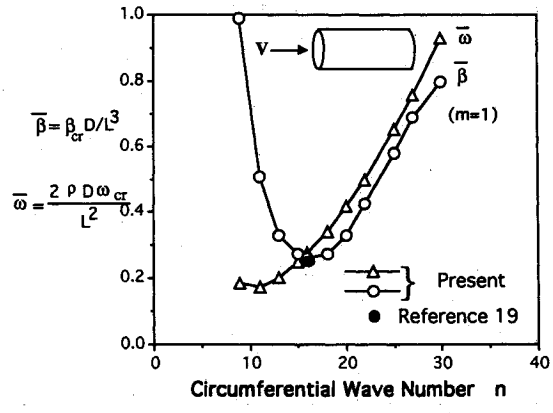

Fig. 6 Flutter boundaries ($\bar{\omega}$ and $\bar{\beta}$) for a simply supported isotropic cylindrical shell with one half longitudinal wave ($m = 1$) and various numbers of full circumferential waves (n).

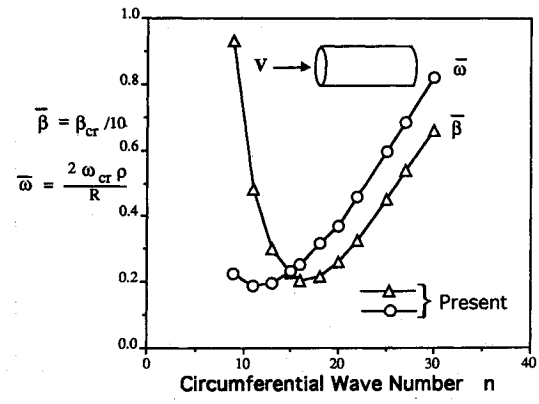

Fig. 7 Flutter boundaries ($\bar{\omega}$ and $\bar{\beta}$) for a laminated $[0/+45/90]_s$ graphite-epoxy composite simply supported cylindrical shell with one half longitudinal wave ($m = 1$) and various numbers of full circumferential waves (n).

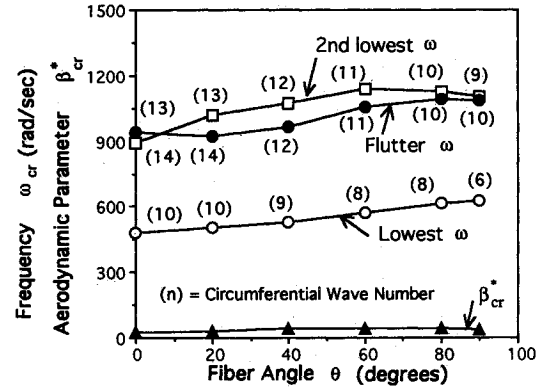

Fig. 8 Effect of fiber orientation (θ) on flutter boundaries (ω_{cr} and β^*_{cr}) for a laminated $[0/\pm\theta/90]_s$ graphite-epoxy composite simply supported cylindrical shell for one half longitudinal wave ($m = 1$).

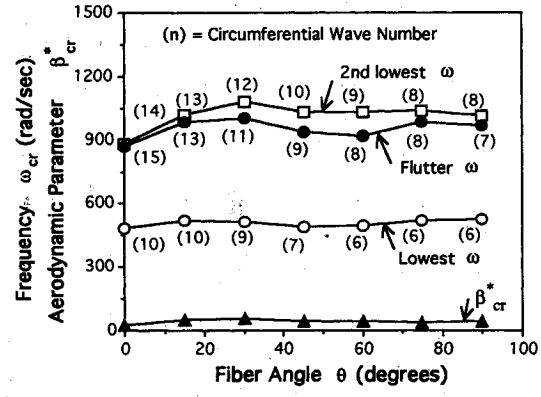

Fig. 9 Effect of fiber orientation (θ) on flutter boundaries (ω_{cr} and β^*_{cr}) for a laminated $[(\pm\theta)_2]_s$ graphite-epoxy composite simply supported cylindrical shell for one half longitudinal wave ($m = 1$).

quencies are given in the parentheses. Each number n was obtained by varying its value until the minimum frequency of interest was found. For example, at $\theta = 20$ deg in Fig. 8, the values of 10, 13, and 14 in the parentheses were found from the plots as shown in Fig. 12a where the minimum values for the two lowest frequencies and the lowest flutter frequency were found by varying the values of n. Such a search was done for each of the θ values. It is seen from Figs. 8–9 and 10–11 that the circumferential wave number in the parentheses decreases along each of the three curves as the fiber angle is increased for the angle-ply laminated cylindrical and conical shells considered, with the exception of the flutter curve at $\theta = 20$ deg in Fig. 8. It is seen that the flutter frequencies ω_{cr} and the circumferential wave numbers n for the flutter curve are all closer to those for the second lowest frequency curve

than those for the lowest frequency curve. In other words, coalescence of the two lowest mode frequencies results in a flutter mode more by the second lowest mode than the lowest mode. The flutter frequency in Fig. 8 is slightly higher than the second lowest frequency at $\theta = 0$ deg, but lower at $\theta = 20$ deg and at higher angles. Although the flutter frequency is higher than the second lowest natural frequency at $\theta = 0$ deg, flutter still occurs when the two lowest modes coalesce. The flutter curve in Fig. 8 shows that the flutter frequency is the smallest at $\theta = 20$ deg and the highest at $\theta = 90$ deg. The values of flutter speed (β^*_{cr}) increase slightly as the fiber angle is increased from $\theta = 10$ deg. Similar trends for ω_{cr} are seen in Fig. 9 for the $[(\pm\theta)_2]_s$ laminated shell. In Fig. 9, the flutter frequency is the smallest at $\theta = 0$ deg and the highest at $\theta = 30$ deg. Then, the values of β^*_{cr} decrease as the fiber angle is increased up to $\theta = 60$ deg, and then go up and down slightly with the increase of θ.

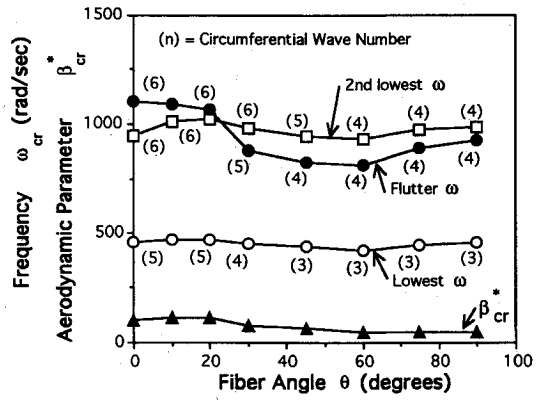

Fig. 10 Effect of fiber orientation (θ) on flutter boundaries (ω_{cr} and β^*_{cr}) for a laminated $[0/\pm\theta/90]_s$ graphite-epoxy composite simply supported 5 deg conical shell for one half longitudinal wave ($m = 1$).

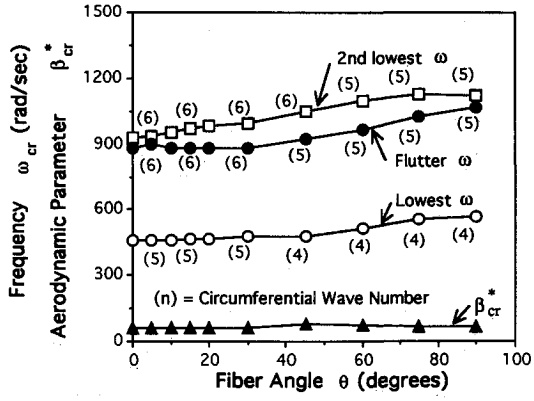

Fig. 11 Effect of fiber orientation (θ) on flutter boundaries (ω_{cr} and β^*_{cr}) for a laminated $[(\pm\theta)_2]_s$ graphite-epoxy composite simply supported 5 deg conical shell for one half longitudinal wave ($m = 1$).

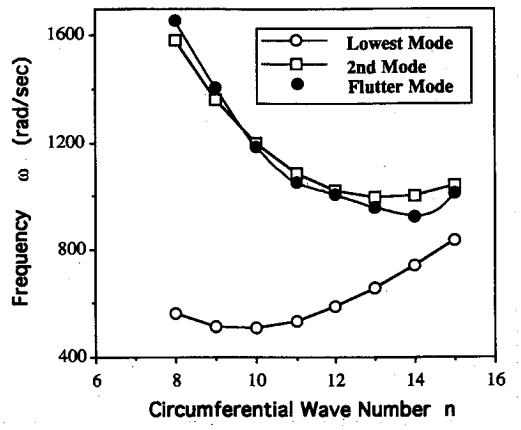

Fig. 12a An example of searching for the circumferential wave numbers in the parentheses in Fig. 8 for $\theta = 20$ deg.

Figure 10 shows that the flutter frequency is the smallest at $\theta = 0$ deg and the highest at $\theta = 90$ deg for the $[0/\pm\theta/90]_s$ conical shell considered. The dynamic pressure parameter β^*_{cr} increases up to $\theta = 45$ deg and then decreases as the fiber angle is increased. For the ten different θ values considered in Fig. 11, the flutter frequencies are higher than the second lowest frequency at θ equal to or smaller than 20 deg, but it is the other way around at θ equal to or higher than 30 deg. It is noted that although the flutter frequencies are higher than the second lowest natural frequencies at $\theta \leq 20$ deg, flutter still occurs when the two lowest modes coalesce. In Fig. 11, the flutter frequency is the smallest at $\theta = 60$ deg and the highest at $\theta = 0$ deg. The values for β^*_{cr} increase up to $\theta = 20$ deg and then decrease as the fiber angle is increased for the $[(\pm\theta)_2]_s$ laminated conical shell. For the present class of simply supported laminated shell problems, modes are mostly obtained by the coalescence of the lowest and the second modes. The flutter mode is usually composed of one longitudinal half-wave and n circumferential full waves, whereas n is equal or close to that of the second free vibration mode. To demonstrate this phenomenon, the flutter modes are shown in Fig. 12b for a cylindrical shell with $m = 1$ and $n = 14$. It can be seen from Figures 8–9 and 10–11 that the circumferential modes and wave numbers n corresponding to flutter are strongly influenced by the laminate fiber angle for the laminated cylindrical and conical shells considered, and the degree of such influence is quantified in the four figures.

Table 3 Examples considered to illustrate the supersonic flutter behavior of isotropic and composite shells with simply supported boundary conditions

Example	Shell type	Layup scheme
1	Cylindrical	Isotropic
2	Conical	Isotropic
3	Cylindrical	$[0/\pm 45/90]_s$
4	Cylindrical	$[0/\pm\theta/90]_s$
5	Cylindrical	$[\pm\theta]_{2s}$
6	Conical	$[0/\pm\theta/90]_s$
7	Conical	$[\pm\theta]_{2s}$
8	Conical	Orthotropic

Table 4 Comparison of flutter dynamic pressure parameter (β^*_{cr}) for an isotropic conical shell with a semivertex angle of 5 deg with simply supported edges (m = 1)

Circumferential wave number (n)	Galerkin method[31]	Reference 20	Present 1 × 10 mesh
4	1074	1082	991
5	590	609	576
6	607	625	620
7	652	695	647

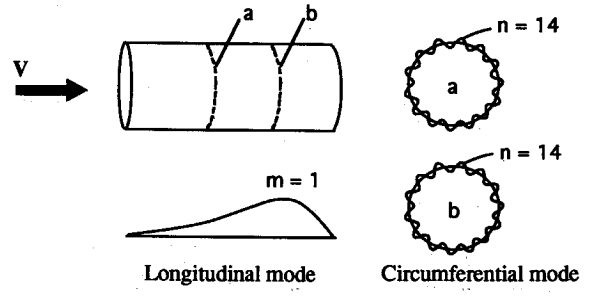

Fig. 12b Flutter mode for $[0/\pm 20/90]_s$ laminated cylindrical shell with longitudinal half wave number $m = 1$ and circumferential wave number $n = 14$.

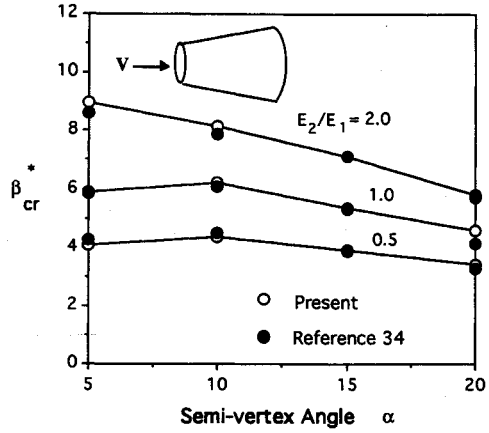

Fig. 13 Effect of orthotropic modulus ratio (E_2/E_1) on flutter aerodynamic parameter (β^*_{cr}) for an orthotropic simply supported conical shell for one half longitudinal wave ($m = 1$) and five circumferential waves ($n = 5$) for four different semivertex cone angles.

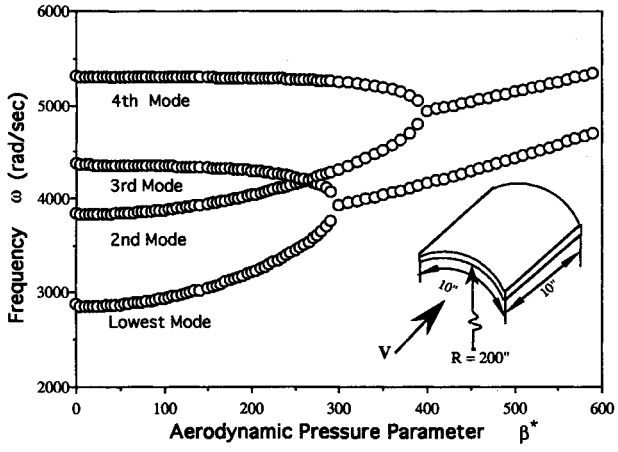

Fig. 14 Coalescence of modes for a [0/90] graphite-epoxy composite cylindrically curved panel with all edges clamped.

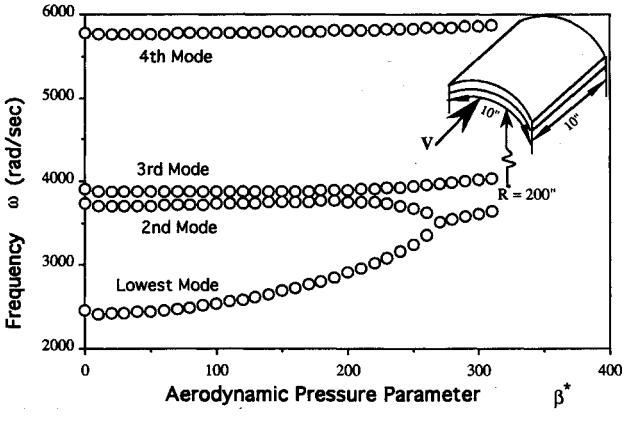

Fig. 15 Coalescence of modes for a [45/−45] graphite-epoxy composite cylindrically curved panel with all edges clamped.

Figure 13 shows the effect of orthotropy (E_2/E_1) for a simply supported orthotropic conical shell. The geometry of the shell is similar to the one used in Table 4. The material properties were assumed as: $E_1 = 6.5 \times 10^6$ psi; $\rho = 0.833 \times 10^{-3}$ lb-sec^2/in,^{4}; and $\nu_{12} = 0.29$. Four different cone semivertex angles of 5 deg, 10 deg, 15 deg, and 20 deg were considered. The results for β^*_{cr} are compared with those obtained by the approximate analytical approach of Librescu.[34] Good agreement is observed. It can be seen that the degree of orthotropy strongly influences β^*_{cr} for a given semivertex angle. The trend of the variation of flutter speed for a given material is influenced by the semivertex angle as quantitatively shown in the three curves in Fig. 13.

Curved Panels

To illustrate the applicability of the present shell finite element formulated for special quadrilateral configurations, the examples of cylindrical and spherical panels with all edges clamped were studied. The geometry of the cylindrical panel was assumed as radius-to-length ratio = 20; length = 10 in,; and thickness $h = 0.01$ in. The geometry of the doubly curved spherical panel was assumed as radius = 200 in. and thickness $h = 0.01$ in. The material properties of ASC/3501-6 graphite-epoxy composite used for both panels were assumed as $E_1 = 21 \times 10^6$ psi; $E_2 = 1.4 \times 10^6$ psi; $G_{12} = 0.6 \times 10^6$ psi;

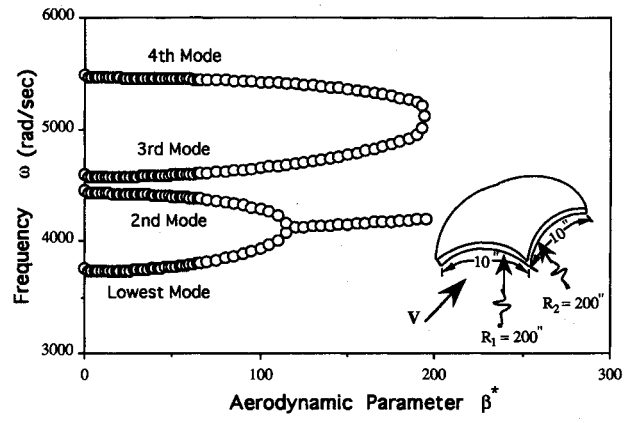

Fig. 16 Coalescence of modes for a [0/90] graphite-epoxy composite spherically curved panel with all edges clamped.

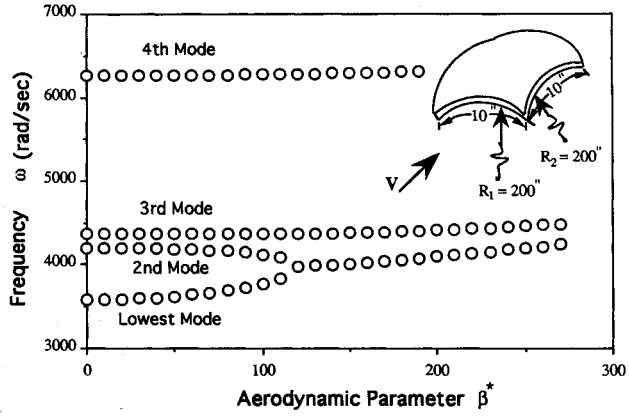

Fig. 17 Coalescence of modes for a [45/−45] graphite-epoxy composite spherically curved panel with all edges clamped.

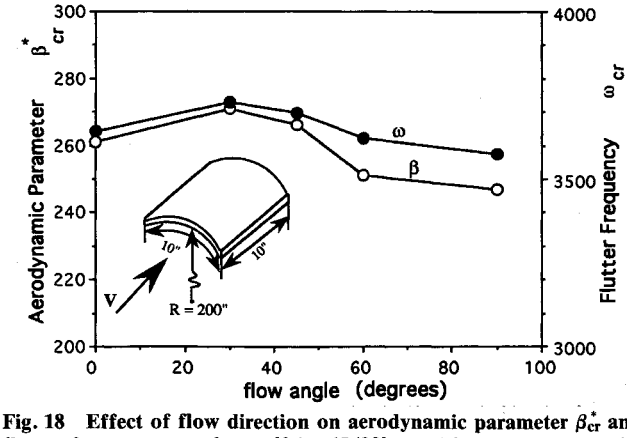

Fig. 18 Effect of flow direction on aerodynamic parameter β^*_{cr} and flutter frequency ω_{cr} for a [0/±45/90] graphite-epoxy composite cylindrical panel with all edges clamped.

Table 5 Comparison of lowest frequency parameters and flutter bounds for the clamped AS4/3501-6 graphite-epoxy cylindrically and spherically curved panels (R = 200 in., a = 10 in., and h = 0.01 in.)

Type of shell	Layup scheme	Lowest frequency (ω^*)		Flutter bounds	
		Present	Reference 35	ω_{cr}	β^*_{cr}
Cylindrical	[0/90]	7.62	7.63	3867	300
Cylindrical	[45/ − 45]	6.53	—	3425	260
Spherical	[0/90]	9.96	9.84	4055	120
Spherical	[45/ − 45]	9.56	—	3927	114

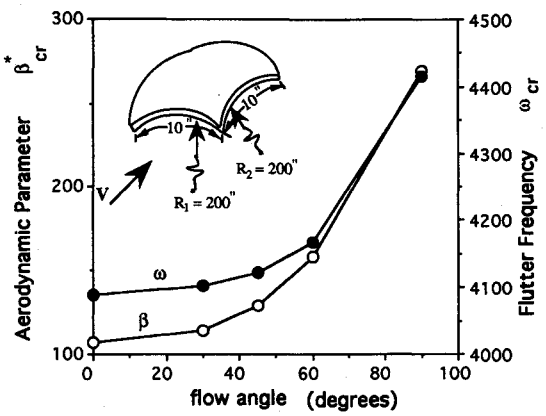

Fig. 19 Effect of flow direction on aerodynamic parameter β^*_{cr} and flutter frequency ω_{cr} for a [0/ ± 45/90] graphite-epoxy composite spherical panel with all edges clamped.

$\rho = 0.1475 \times 10^{-3}$ lb-sec^2/in.^{4}; and $\nu_{12} = 0.3$. The results for the lowest natural frequency parameter ω, flutter frequency ω_{cr}, and dynamic pressure parameter β^*_{cr} for a [0/90] and a [45/ − 45] laminated cylindrical panel as well as a [0/90] and a [45/ − 45] laminated spherical panel are shown in Table 5. The natural frequency parameters agree well with those given by Chandrashekhara[35] for the [0/90] laminated cylindrical and spherical panels.

The phenomena of coalescences of modes for the cylindrical and spherical panels laminated with [0/90] and [45/ − 45] schemes are shown in Figs. 14–15 and 16–17, respectively. Figure 14 shows that, for the [0/90] laminated cylindrical panel, the flutter mode is caused by the coalescence of modes 1 and 3. It is of interest to see that, when the fiber angles are changed to [45/ − 45], the flutter mode is caused by the coalescence of modes 1 and 2 as shown in Fig. 15. It is seen from Figs. 16 and 17 that for the [0/90] and [45/ − 45] laminated spherical panels, the critical flutter is caused by the coalescence of modes 1 and 2 for both cases. It is interesting to observe from the plots of Figs. 14–17 the effect of fiber orientation on the phenomenon of coalescence of modes. The critical flutter does not necessarily occur by the coalescence of the two lowest modes.

Figures 18 and 19 show the effect of flow angle on the flutter aerodynamic pressure parameter β_{cr} and flutter frequency ω_{cr} for a [0/ ± 45/90] laminated cylindrical panel and a [0/ ± 45/90] spherical panel, respectively. For the five different flow angles considered for the cylindrical panel as shown in Fig. 18, the flutter frequency and aerodynamic parameter increase up to a flow angle of 30 deg and then decrease as the flow angle is increased. In Fig. 19, for the spherical panel considered, both the β^*_{cr} and ω_{cr} increase as the flow angle is increased from 0 deg to 90 deg. It can be seen from Figs. 18 and 19 that flow direction has a strong influence on flutter frequency for laminated cylindrical and spherical panels, and the degree of such influence is quantified here.

IV. Concluding Remarks

A supersonic flutter analysis of laminated composite plates and shells is carried out using a doubly curved quadrilateral thin shell finite element, developed on the basis of the Kirchhoff-Love thin shell theory, classical lamination theory, and linear piston aerodynamic theory. Numerical results are obtained for laminated composite plates and curved panels, and isotropic and composite cylindrical and conical shells. Good agreement of some of the obtained solutions with existing results serves to establish the validity of the present formulations for supersonic flutter analysis of laminated composite plates and shells. The present results quantitatively illustrate the effects of flow angle, boundary conditions, orthotropy, and fiber orientation on the flutter bounds and mode shapes. The present results show quantitatively the relations among the fundamental natural frequencies and flutter frequencies and their corresponding circumferential modes for the selected examples of the composite cylindrical shells and conical shells. The results presented illustrate the phenomenon of coalescent mode shifting due to the change of fiber orientations for the curved composite panels. The presented results indicate that fiber angle and orthotropy strongly influence the flutter boundaries for laminated cylindrical shells, conical shells, and curved panels. Such influences are quantified in the present examples, and physical interpretations are made. It is noted that, in addition to demonstrating the applicability of the present curved quadrilateral thin shell finite elements for panel flutter, it would be useful to study the effects of real world problems of angle of attack and aerodynamic heating. When such effects are included in the analysis, more interesting and accurate results can be obtained, and this is a topic worthy of further study. Currently, research is being done to explore the effect of aerodynamic heating. Extensions can also be made to include aerodynamic and structural nonlinearities.

References

[1]Fung, Y. C., *The Theory of Aeroelasticity,* Wiley, New York, 1955.

[2]Bisplinghoff, R. Y., and Ashley, H., *Principles of Aeroelasticity,* Dover, New York, 1962.

[3]Dowell, E. H., *Aeroelasticity of Plates and Shells,* Noordhoff International, Leyden, The Netherlands, 1975.

[4]Dowell, E. H., Curtiss, H. C., Jr., Scanlan, R. H., and Sisto, F., *A Modern Course in Aeroelasticity,* Sijthoff & Noordhoff, The Netherlands, 1978.

[5]Fung, Y. C., "Some Recent Contributions to Panel Flutter Research," *AIAA Journal,* Vol. 1, No. 4, 1963, pp. 898–909.

[6]Dowell, E. H., "Panel Flutter: A Review of the Aeroelastic Stability of Plates and Shells," *AIAA Journal,* Vol. 8, No. 3, 1970, pp. 385–399.

[7]Olson, M. D., "Some Flutter Solutions Using Finite Elements," *AIAA Journal,* Vol. 8, No. 4, 1970, pp. 747–752.

[8]Sander, G., Bon, C., and Geradin, M., "Finite Element Analysis of Supersonic Panel Flutter," *International Journal for Numerical Methods in Engineering,* Vol. 7, No. 3, 1973, pp. 379–394.

[9]Yang, T. Y., and Sung, S. H., "Finite Element Flutter in Three-dimensional Supersonic Unsteady Potential Flow," *AIAA Journal,* Vol. 15, No. 12, 1977, pp. 1677–1683.

[10]Mei, C., "A Finite Element Approach for Non-linear Panel Flutter," *AIAA Journal,* Vol. 15, No. 8, 1977, pp. 1107–1110.

[11]Ketter, D. J., "Flutter of Flat, Rectangular, Orthotropic Panels," *AIAA Journal,* Vol. 8, No. 2, 1967, pp. 116–124.

[12]Rossettos, J. N., and Tong, P., "Finite Element Analysis of Vibration and Flutter of Cantilever Anisotropic Plates," *Journal of Applied Mechanics,* ASME, Vol. 41, No. 4, 1974, pp. 1075–1080.

[13]Srinivasan, R. S., and Babu, B. J., "Free Vibration and Flutter of Laminated Quadrilateral Plates," *Computers and Structures,* Vol. 27, No. 2, 1987, pp. 297–304.

[14]Lin, K. J., Lu, P. J., and Tam, J. Q., "Flutter Analysis of Composite Panels Using High-Precision Finite Elements," *Computers and Structures,* Vol. 33, No. 2, 1989, pp. 561–574.

[15]Sawyer, J. W., "Flutter and Buckling of General Laminated Plates," *Journal of Aircraft,* Vol. 14, No. 4, 1977, pp. 387–393.

[16]Oyibo, G. A., "Flutter of Orthotropic Panels in Supersonic Flow using Affine Transformations," *AIAA Journal,* Vol. 21, No. 3, 1983, pp. 283–289.

[17]Olson, M. D., and Fung, Y. C., "Comparing Theory and Experiment for the Supersonic Flutter of Circular Cylindrical Shells," *AIAA Journal,* Vol. 5, No. 10, 1967, pp. 1849–1856.

[18]Matsuzaki, Y., and Kobayashi, S., "Nonlinear Analysis of Super-

sonic Panel Flutter of Circular Cylindrical Shells," *Transactions of Japan Society for Aeronautical and Space Sciences,* Vol. 18, No. 194, 1970, pp. 103–111.

[19]Kobayashi, S., "Supersonic Panel Flutter of Unstiffened Circular Cylindrical Shells having Simply Supported Ends," *Transactions of Japan Society for Aeronautical and Space Sciences,* Vol. 6, No. 9, 1963, pp. 27–35.

[20]Ueda, T., Kobayashi, S., and Kihira, M., "Supersonic Flutter of Truncated Conical Shells," *Transactions of Japan Society for Aeronautical and Space Sciences,* Vol. 20, No. 47, 1977, pp. 13–30.

[21]Bismarck-Nasr, M. H., "Finite Element Method Applied to the Supersonic Flutter of Circular Cylindrical Shells," *International Journal for Numerical Methods in Engineering,* Vol. 10, No. 2, 1976, pp. 423–435.

[22]Bismarck-Nasr, M. H., "Finite Element Solution of the Supersonic Flutter of Conical Shells," *AIAA Journal,* Vol. 17, No. 10, 1979, pp. 1148–1150.

[23]Sunder, P. J., Ramakrishnan, C. V., and Sengupta, S., "Finite Element Analysis of 3-Ply Laminated Conical Shell for Flutter," *International Journal for Numerical Methods in Engineering,* Vol. 19, No. 8, 1983, pp. 1183–1192.

[24]Olson, M. D., and Fung, Y. C., "Supersonic Flutter of Circular Cylindrical Shells Subjected to Internal Pressure and Axial Compression," *AIAA Journal,* Vol. 4, No. 5, 1966, pp. 858–864.

[25]Carter, L. L., and Stearman, R. O., "Some Aspects of Cylindrical Shell Panel Flutter," *AIAA Journal,* Vol. 6, No. 1, 1968, pp. 37–43.

[26]Matsuzaki, Y., "Natural Vibration and Flutter of Cylindrically Curved Panels," *AIAA Journal,* Vol. 11, No. 6, 1973, pp. 771–772.

[27]Yang, T. Y., "High-order Rectangular Shallow Shell Finite Elements," *Journal of Engineering Mechanics Division,* ASCE, Vol. 99, No. EM1, 1973, pp. 157–181.

[28]Jones, R. M., *Mechanics of Composite Materials,* McGraw-Hill, New York, 1975.

[29]Lighthill, M. J., "Oscillating Airfoils at High Mach Number," *Journal of Aerospace Sciences,* Vol. 20, No. 6, 1953, pp. 402–406.

[30]Voss, H. M., "The Effect of an External Supersonic Flow on the Vibration Charateristics of Thin Cylindrical Shells," *Journal of Aerospace Sciences,* Vol. 12, No. 12, 1961, pp. 945–956.

[31]Dixon, S. C., and Hudson, M. L., "Flutter, Vibration, and Buckling of Truncated Orthotropic Conical Shells with Generalized Elastic Edge Restraint," NASA TN D-5759, 1970.

[32]Thorton, E. A., and Clary, R. R., "Correlation study of Finite Element Modeling for Vibrations of Composite Material Panels," *In Composite Materials: Testing and Design,* American Society for Testing and Materials STP 546, 1974, pp. 111–129.

[33]Lee, In., and Cho, M. H., "Flutter Analysis of Composite Panels in Supersonic Flow," *Proceedings of the AIAA/ASME/ASCE/AHS/ASC 31st Structures, Structural Dynamics, and Materials Conference* (Long Beach, CA), AIAA, Washington, DC, April 1990 (AIAA Paper 90-1180).

[34]Librescu, L., *Elastostatics and Kinetics of Anisotropic and Heterogeneous Shell Type Structures,* Noordhoff International, Leyden, The Netherlands, 1975.

[35]Chandrashekhara, K., "Free Vibrations of Anisotropic Laminated Doubly Curved Shells," *Computers and Structures,* Vol. 33, No. 2, 1989, pp. 435–440.